Journal of Power Sources 183 (2008) 406–410

Contents lists available at ScienceDirect

Journal of Power Sources

journal homepage: www.elsevier.com/locate/jpowsour

Short communication

Significantly enhanced charge conduction in electric double layer capacitors using carbon nanotube-grafted activated carbon electrodes

Cheng-Wei Huang[a,1], Chih-Ming Chuang[b,1], Jyh-Ming Ting[b], Hsisheng Teng[a,*]

[a] Department of Chemical Engineering and Center for Micro/Nano Science and Technology, National Cheng Kung University, Tainan 70101, Taiwan
[b] Department of Materials Science and Engineering, National Cheng Kung University, Tainan 70101, Taiwan

ARTICLE INFO

Article history:
Received 31 January 2008
Received in revised form 26 April 2008
Accepted 30 April 2008
Available online 7 May 2008

Keywords:
Conductivity enhancement
Double layer capacitance
Carbon nanotube
Activated carbon fiber
Electrochemical capacitor
Nanotube grafting

ABSTRACT

Carbon nanotube (CNT)-grafting by chemical vapor deposition was conducted to reduce the resistance of activated carbon fiber serving as an electrode for electric double layer capacitors. Sputtering deposition of Ni catalyst particles led to a uniform growth of CNTs on the carbon fiber surface through the tip-growth mechanism. Because sputtering deposition ensures little pore blockage (in comparison with wet-impregnation), the surface area decrease of the carbon fiber due to Ni loading was minimized. By using H_2SO_4 aqueous solution as the electrolyte, a capacitor cell assembled with the CNT-grafted fiber showed higher electron and electrolyte-ion conductivities relative to a cell assembled with the bare fiber. By increasing the discharging current density from 1 to 150 mA cm^{-2}, the bare fiber exhibited a capacitance loss of 17% while the CNT-grafted fiber showed a mitigated capacitance loss of only 7%. This developed CNT-grafting technique renders activated carbon fiber a promising electrode material for a variety of electrochemical applications.

1. Introduction

Electric double layer capacitors (EDLCs) with high-energy density were developed by taking advantage of the large surface area of porous carbon materials [1–18]. Because of the physical nature of the double layer formation mechanism, these EDLCs are provided with high power density and long cycle life. In practical applications, it requires a special attention on the minimization of energy dissipation due to electron or electrolyte-ion transport [17–26]. Decreasing the resistance within EDLCs is, in fact, the key to enhance the energy storage efficiency.

The resistance within an EDLC results mainly from the electrical contact resistance in electrodes, the resistance in the solution bulk phase, and the resistance of ion migration in the carbon micropores [5,9,21]. Activated carbon fibers, which contain micropores opening directly to the outer surface, are considered an appropriate electrode material for EDLCs [27–30]. The high accessibility of the micropores significantly minimizes the ion transport restriction and thus promotes the double layer build-up on carbon surface. To achieve high-energy storage per unit electrode area, a carbon film of a considerably large thickness is essentially required to fabricate EDLCs. Under this circumstance, the internal resistance of the carbon electrode itself becomes an issue of great importance. Activated carbon fibers have their sheaths composed of the basal planes of the graphite crystallites [27]. This has induced a large electrical contact resistance between the fiber threads and thus restricted the application of this carbon material for EDLCs aimed at high power densities.

Carbon nanotubes (CNTs) are known to have high electrical conductivity and chemical stability [31–38]. These features render CNTs an ideal additive for electrodes to improve the conductivity [39–45]. In the present work we develop a technique to grow CNTs on a polyacrylonitrile (PAN)-based activated carbon fiber, in an attempt to enhance the electronic conductivity between the constituting fiber threads. For EDLCs assembled with this carbon fiber, the CNT-grafting modification is shown to significantly enhance the conduction of both electrons and electrolyte-ions during double layer formation.

2. Experimental

The PAN-based activated carbon fiber used was in the form of woven cloth, having a thickness of 0.4–0.6 mm, Brunauer–Emmett–Teller (BET) surface area of 1200 $m^2 g^{-1}$, and pore volume of 0.59 $cm^3 g^{-1}$. We used nickel as the catalyst for the growth of CNTs on the carbon cloth. The catalyst was deposited on carbon cloth (6 cm × 6 cm) using sputtering deposition, in which

* Corresponding author. Tel.: +886 6 2385371; fax: +886 6 2344496.
E-mail address: hteng@mail.ncku.edu.tw (H. Teng).
[1] These authors contributed equally to this work.

0378-7753/$ – see front matter © 2008 Elsevier B.V. All rights reserved.
doi:10.1016/j.jpowsour.2008.04.075

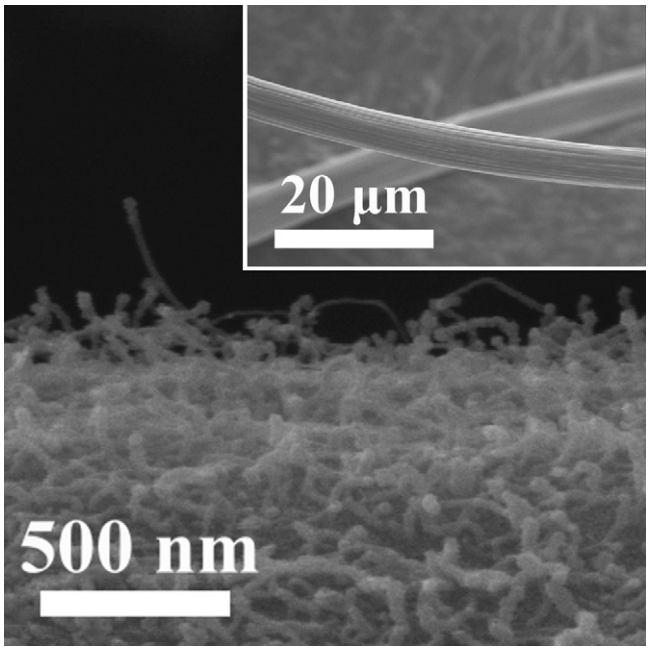

Fig. 1. SEM image of the activated carbon fiber grafted with carbon nanotubes. The inset shows the image of fiber threads constituting the bare activated carbon fiber.

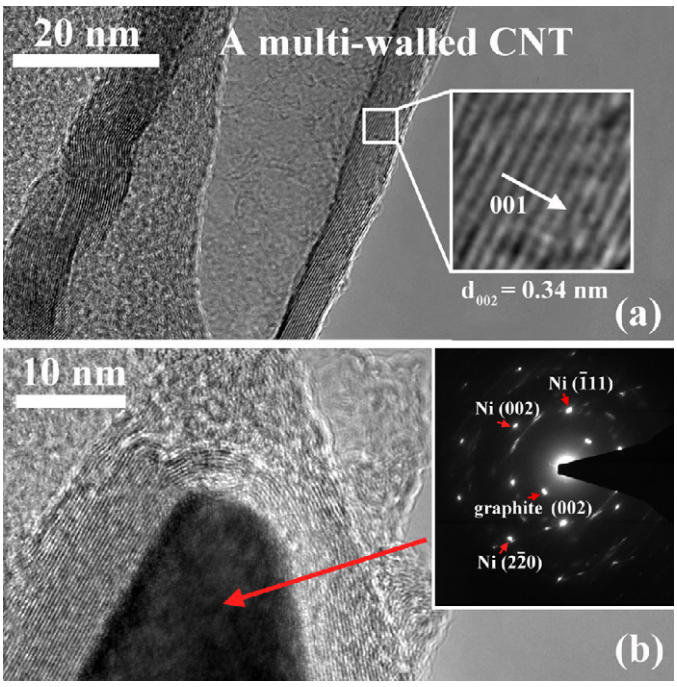

Fig. 2. TEM images of a carbon nanotube grown on the activated carbon fiber: (a) the center portion of the tube; (b) the end portion of the tube with the selected area electron diffraction pattern shown in the inset. The electron diffraction pattern is obtained with the incident beam directing along the Ni [1 1 0] and graphite [0 1 0] directions.

the nickel target was of 99.99% in purity. The deposition was performed for 5 min at a working pressure of 5×10^{-2} Torr, an argon flow rate of 15 cm^3 min^{-1}, a radio-frequency power of 50 W, and an electrode distance of 5 cm. After the catalyst seeding, CNTs were grown on the cloth using a thermal chemical vapor deposition method. Prior to the growth, the catalyst on the cloth was treated with H_2 (1 atm) at 400 °C for 1 h. The growth of CNTs was performed at 800 °C for 1 h under atmospheric pressure, using methane as the carbon source and hydrogen as the balance gas at a CH_4/H_2 ratio of 3/17. The CNTs grown on the carbon cloth were analyzed with scanning electron microscopy (SEM; JEOL JSM-6700F), transmission electron microscopy (TEM; Hitachi FE-2000), and Raman spectroscopy (Renishaw; 10 mW He–Ne laser, 633 nm in wavelength).

Two-electrode cells were used to examine the electrochemical performance of the carbon fiber specimens. The electrode of the cells consisted of 1 cm^2 carbon cloth and stainless-steel foil as the current collector. The cells were constructed with a pair of the electrodes sandwiching a cellulose fiber filter paper as separator. All electrochemical measurements were carried out using 2 M H_2SO_4 as electrolyte at the ambient temperature. Galvanostatic charge–discharge was used to determine the capacitance of the electrodes. An ac impedance spectrum analyzer combined with a computer software was employed to measure and analyze the impedance behavior of the cells. The impedance measurements were conducted at 0 V with an ac potential amplitude of 5 mV and a frequency range of 10 mHz–100 kHz.

3. Results and discussion

Fig. 1 shows the external feature of the activated carbon fiber grafted with CNTs. The SEM image shows that CNTs were uniformly grown on the fiber surface with a population density of $2–6 \times 10^9$ cm^{-2}. The inset of Fig. 1 shows the image of bare fiber threads, which have a diameter of ca. 7 μm. A large majority of the CNTs grown on the fiber had an average tube diameter of 40–50 nm. This requires a uniform size of Ni nanoparticles deposited on the carbon fiber. We deposited these Ni particles with the sputtering method to avoid the blockage of micropores in the activated carbon. Wet chemical-impregnation for catalyst loading, on the other hand, leads to serious pore blockage in most cases. The CNT-grafted carbon fiber had a BET surface area only slightly smaller than the bare fiber (1160 m^2 g^{-1} vs. 1200 m^2 g^{-1}).

Another advantage of the sputtering method is to form a weak interaction between the catalyst and carbon substrate. The weak interaction would lead to the "tip-growth" mode for CNT formation. The tip-growth mode is preferred here because it would create a direct electrical connection between the grafted CNTs and the fiber surface. The typical TEM image of the CNTs grafted on the fiber is depicted in Fig. 2. Fig. 2(a) shows the center portion of a CNT. The image clearly demonstrates the multi-walled feature of the CNTs grafted on the fiber. For a large majority of the CNTs, the graphene layers are well orientated and parallel to the tube axis, as shown in the inset. The tube wall has an average d_{002} spacing of 0.342 nm, which is larger than that of pure graphite (0.335 nm). However, in some CNTs there are graphene layers that tilt and truncate, as depicted by the left-hand wall of the CNT in Fig. 2(a).

Fig. 2(b) shows the appearance of an encapsulated catalyst particle at the end of the CNT, in agreement with the anticipated tip-growth mode. This catalyst particle has well-defined crystalline structure, as reflected by the selected area electron diffraction pattern shown in the inset of Fig. 2(b). The diffraction points can be indexed according to the face-centered cubic structure of metallic Ni ($Fm\bar{3}m$, space group no. 225, with a = 3.523 Å; JCPDS 87-0712) with a zone axis directing along the [1 1 0] direction. The pattern also records the diffraction from graphite with a zone axis directing along graphite [0 1 0]. The graphite structure is assigned to the CNT endcap encapsulating the catalyst particle. Because the structure of nickel metal, rather than nickel carbide, was detected by the diffraction analysis, surface diffusion of carbon around the Ni particle should be the mechanism in this catalytic growth of CNTs. In the electron diffraction pattern shown in Fig. 2(b), the diffraction

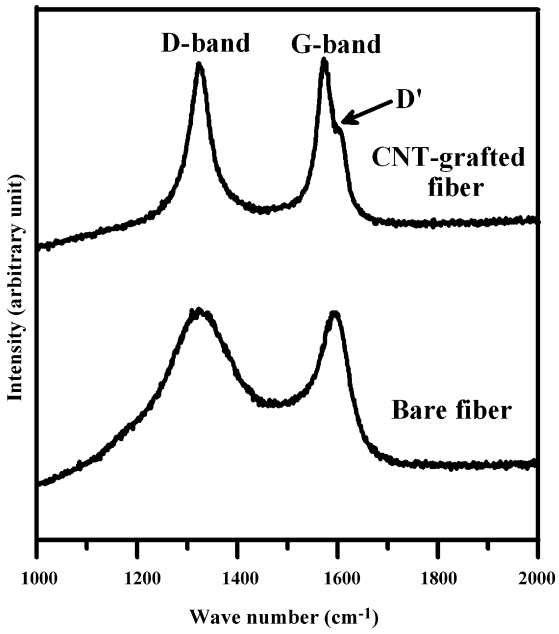

Fig. 3. Raman spectra of the bare and CNT-grafted carbon fibers.

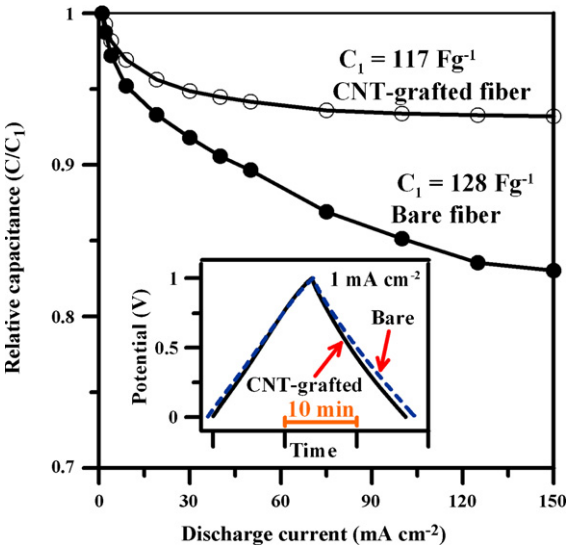

Fig. 4. Variation of the relative capacitance (C/C_1) with discharge current for the bare and CNT-grafted fibers serving as electrodes for EDLCs. The relative capacitance was obtained by dividing the specific capacitance (C) with the value obtained at 1 mA cm^{-2} (C_1). The EDLCs have been charged to 1 V prior to discharge. The inset shows typical potential-against-time curves of the EDLCs charged and discharged at 1 mA cm^{-2}.

center and the graphite (0 0 2) and Ni(2 $\bar{2}$ 0) diffraction spots can be connected by a straight line. This reflects that the graphite [0 0 2] direction is parallel to the [1 1 0] direction of Ni. It was reported that the Ni(1 1 0) face is active for methane dissociation, while unfavorable for graphite binding [46,47]. Under this circumstance, it is likely that in the CNT growth the carbon atoms from methane dissociation diffuse on the Ni(1 1 0) plane and are incorporated into the new graphene layers at the edge of the (1 1 0) plane. This mechanism explains how the nanotubes were grown in the tip-growth mode with their graphene layers parallel to the Ni(1 1 0) plane.

The chemical structure of the bare and CNT-grafted carbon fibers was analyzed with Raman spectroscopy. Fig. 3 compares the Raman signatures of these carbon fibers. Both carbon specimens show well-defined D- and G-band peaks in the spectra. For the most part, the D-band is observed at 1350 cm^{-1} and G-band at 1580 cm^{-1} for carbons. The G-band corresponds to a phonon high-frequency E_{2g} first-order mode of graphite and is related to the vibration of sp^2-bonded carbon atoms in a two-dimensional hexagonal lattice, such as in a graphite sheet [48–51]. On the other hand, the D-band results from vibrations of carbon atoms with dangling bonds in crystal lattice plane terminations of disordered graphite or defects in the curved graphene sheets. The intensity ratio of the D- to G-band, I_D/I_G, can be used to estimate the quality of carbon materials. The obtained I_D/I_G values here were 1.0 and 0.98 for the bare and CNT-grafted fibers, respectively. The similarity in I_D/I_G reflects that the overall crystallinity, which affects the conductivity, remained similar after the introduction of CNTs. However, there is a shoulder peak at ~1600 cm^{-1} (D′ peak) on the G-band of the CNT-grafted fiber. This D′ peak is induced by disorders resulting from the finite size effect or lattice distortion [49–51], which are characteristics of multi-walled CNTs. It is obvious that the D′ peak is contributed by multi-walled feature of the CNTs grafted on the fiber.

A constant current charge–discharge cycling was conducted to measure the capacitance of capacitor cells assembled with the bare and CNT-grafted fibers. The specific discharge capacitance (C) of the electrodes in the cells was calculated according to

$$C = \frac{(2 \times i \times t)}{(W \times \Delta E)} \quad (1)$$

where i is the discharge current, t the discharge time, W the carbon fiber mass of an electrode, and ΔE the potential difference in discharge, excluding the portion of IR drop. The factor of 2 comes from the total capacitance measured from the two-electrode cells being the addition of two equivalent single-electrode capacitors in series. The potential-against-time curves of the bare and CNT-grafted fibers charged and discharged at 1 mA cm^{-2} are depicted in the inset of Fig. 4, showing a standard capacitive behavior for both fibers. The times required for charge or discharge for the two cells were almost identical at this low current density, reflecting similar ultimate charge-storage capacities. Fig. 4 shows the variation of the relative capacitance (C/C_1; C_1 = the ultimate capacitance obtained at 1 mA cm^{-2}) with the discharge current density. The relative capacitance is equivalent to the rate capability of an EDLC [22]. The C_1 values are similar for these two carbon fiber specimens. For each carbon specimen the relative capacitance deviates from unity with discharge current, suggesting the intrusion of cell resistance in the charge-storage process. It is of interest to observe that the capacitance decrease with current for the CNT-grafted fiber is less dramatic relative to that for the bare fiber. At a high discharge current of 150 mA cm^{-2}, the relative capacitance decreases to 83% for the bare fiber while it stays at a value as high as 93% for the CNT-grafted fiber. The CNT-grafting must have significantly mitigated the charge resistance of a cell assembled with the carbon fiber.

The durability of the capacitor cells should be concerned as well. Both the bare and CNT-grafted carbon fibers showed stable capacitance and high coulombic efficiency (above 99%) over 100 cycles of charge–discharge between 0 and 1 V at 1 mA cm^{-2}. The residual Ni catalyst had little influence on the durability of the resulting EDLCs. This can be partially attributed to the fact that the encapsulated Ni catalyst was well protected by the CNT endcaps, as shown in Fig. 2(b).

Ac impedance spectroscopy, which distinguishes the resistance and capacitance of a device, was employed to analyze the resistance components regarding the double layer formation on the fiber electrodes. The impedance spectra scanned at 0 V are shown in Fig. 5(a) as a Nyquist plot. Fig. 5(b) and (c) shows the magnification of the high-frequency region of the impedance spectra for the

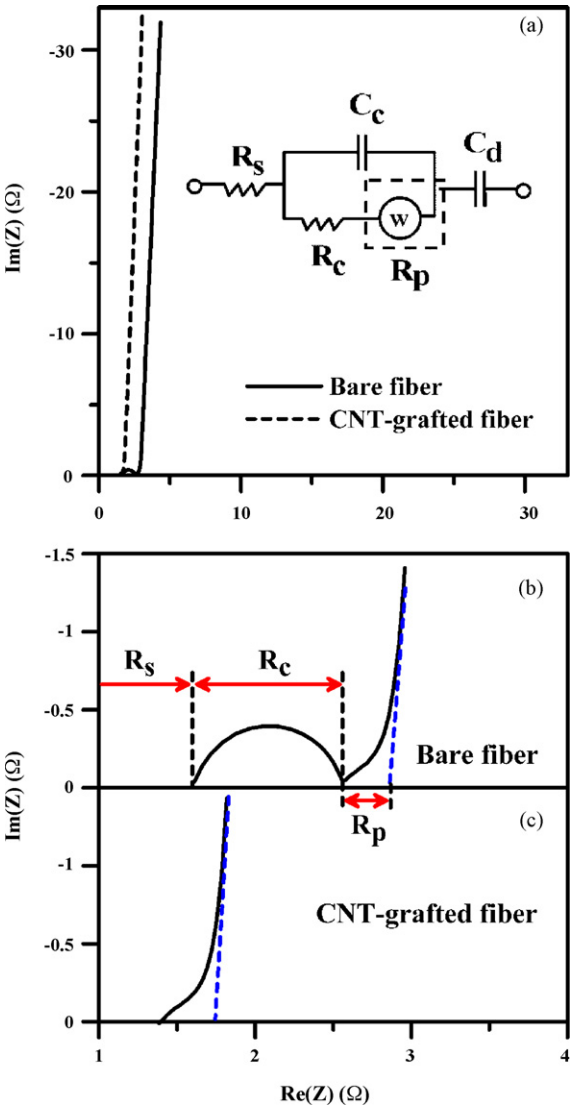

Fig. 5. (a) Nyquist impedance plots of the EDLC cells assembled with the bare and CNT-grafted fibers with the frequency ranging from 10 mHz to 100 kHz at an applied potential of 0 V; (b) the magnification of the high-frequency region of the impedance spectra for the cell assembled with the bare fiber; (c) the magnification of the high-frequency region of the impedance spectra for the cell assembled with the CNT-grafted fiber. The equivalent circuit for the impedance data is shown in the set of (a). In the circuit C_c is the capacitance due to the contact interface, C_d the capacitance inside pores and w a Warburg diffusion element.

two cells. For the bare fiber there is a semicircle intersecting the real axis in the high-frequency region. The locus of the semicircle intercepts the Re(Z) axis at R_s and $R_s + R_c$ in the Nyquist plot, where R_c represents the electrical contact resistance of the electrode and R_s the resistance of ion migration in the bulk solution. The values of R_s and R_c for the cell assembled with the bare fiber were thus obtained from the intercepts in the Nyquist plot shown as Fig. 5(b). Following the semicircle with decreasing frequency, the plot for the bare fiber transforms to a vertical line with the presence of a transition zone. The transition is a consequence of the distributed resistance/capacitance in the carbon micropores [2,4]. An equivalent circuit for the capacitor cells is shown in the inset of Fig. 5(a). A Warburg diffusion element is incorporated in the circuit to emphasize the distributed resistance for ion diffusion in the micropores. As shown in Fig. 5(b), the extrapolation of the vertical line intercepts the Re(Z) axis at R_t ($=R_s + R_c + R_p$), where R_t is the total resistance

Table 1
Components of the EDLC resistance determined from the impedance spectra shown in Fig. 5(b) and (c) for the cells assembled with the bare and CNT-grafted activated carbon fibers

Carbon type	R_t (Ω)	R_s (Ω)	R_c (Ω)	R_p (Ω)
Bare	2.9	1.6	0.97	0.32
CNT-grafted	1.8	1.4	0.00	0.40

The total resistance (R_t) equals to the sum of the resistance of ion migration in the bulk solution (R_s), internal contact resistance of the electrode (R_c) and equivalent distributed pore resistance (R_p).

and R_p the equivalent distributed pore resistance [4]. We obtained the value of R_t from the extrapolated intercept on the Re(Z) axis and determined the value of R_p by subtracting R_s and R_c from R_t. Table 1 summarizes the values of all the resistance components for the cell assembled with the bare fiber.

As to the cell assembled with the CNT-grafted fiber, there is no semicircle observed for the impedance Nyquist plot shown in Fig. 5(a) and (c). This indicates that the internal resistance in the carbon fiber electrode was eliminated as a result of the grafting of CNTs on the fiber surface. The resistance components determined from the impedance data in Fig. 5(c) are also listed in Table 1 to compare with those for the bare fiber cell. The cell assembled with the CNT-grafted fiber had a smaller total resistance than the cell with the bare fiber, i.e. 1.8 Ω vs. 2.9 Ω. The difference in the cell resistance is principally contributed by the elimination of the internal contact resistance in the electrode. Table 1 shows that the internal contact resistance of the bare fiber was reduced from 0.97 to 0.00 Ω by the CNT grafting.

In addition, the cell assembled with the CNT-grafted fiber showed a smaller R_s value. It is possible that the CNT grafting has led to a more intimate contact of the electrolyte solution with carbon fiber to facilitate the transport of ions and solvent molecules. The presence of CNTs may have increased the overlapping potential of the carbon surface and thus enhanced the affinity of the fiber surface for the electrolyte solution. The ruptured spots on the CNT surface, as shown in Fig. 2(a), are polar in nature and can promote the affinity for the electrolyte. There is also a possibility that the smaller R_s of the CNT-grafted fiber was caused by the reduced electrode resistance. Because of the grafting of the highly conductive CNTs, the polarization rate at the solid/solution interface would be significantly promoted. This polarization promotion would give a smaller value for R_s, which corresponds to the cell resistance detected at high ac frequencies. Obviously, the CNT-growth technique developed in the present work not only bridges the gap between the carbon fibers for electron conduction, but also creates for the fiber surface a boundary layer that facilitates interface polarization.

4. Conclusions

The internal resistance of carbon fiber electrodes with a considerably large thickness can be significantly reduced by grafting CNTs on the fiber surface. To graft CNTs on activated carbon fiber in the present work, Ni catalyst particles were uniformly deposited on the fiber by using a sputtering method, which showed little blockage of the micropores in the activated carbon. The weak interaction between the deposited Ni and carbon substrate has led to the "tip-growth" mode for CNT formation, thus creating a direct electrical connection between the grafted CNTs and the fiber surface. The graphene layers of the CNT endcap were found to be parallel to the (1 1 0) plane of the Ni catalyst. Because of this CNT grafting the electrical conductivity between the fiber threads was significantly enhanced. Using the carbon fiber as electrodes for EDLCs, the resis-

tance of the electrolyte-ion motion was also reduced as a result of this CNT grafting. The introduction of the CNTs may have formed an intimate contact between the electrolyte solution and carbon surface, or have promoted the solid/solution interface polarization. Consequently, carbon fibers grafted with CNTs, with the catalyst deposited by sputtering, can serve as an EDLC electrode with low energy loss, especially for operation with speedy charge–discharge.

Acknowledgements

This research was supported by the National Science Council of Taiwan (NSC 96-2120-M-006-006) and the Center for Micro/Nano Science and Technology of National Cheng Kung University.

References

[1] K. Kinoshita, Carbon: Electrochemical and Physicochemical Properties, John Wiley & Sons, New York, 1988, pp. 293–387.
[2] B.E. Conway, Electrochemical Supercapacitors Scientific Fundamentals and Technological Applications, Kluwer Academic, New York, 1999, pp. 105–220.
[3] T. Osaka, X. Liu, M. Nijima, T. Momma, J. Electrochem. Soc. 146 (1999) 1724–1729.
[4] R. Kötz, M. Carlen, Electrochim. Acta 45 (2000) 2483–2498.
[5] S. Yoon, J. Lee, T. Hyeon, S.M. Oh, J. Electrochem. Soc. 147 (2000) 2507–2512.
[6] E. Frackowiak, F. Béguin, Carbon 39 (2001) 937–950.
[7] M. Endo, T. Maeda, T. Takeda, Y.J. Kim, K. Koshibak, H. Hara, J. Electrochem. Soc. 148 (2001) A910–A914.
[8] C.T. Hsieh, H. Teng, Carbon 40 (2002) 667–674.
[9] Y.R. Nian, H. Teng, J. Electrochem. Soc. 149 (2002) A1008–A1014.
[10] D. Lozano-Castelló, D. Cazorla-Amorós, A. Linares-Solano, S. Shiraishi, H. Kurihara, A. Oya, Carbon 41 (2003) 1765–1775.
[11] Y. Soneda, M. Toyoda, K. Hashiya, J. Yamashita, M. Kodama, H. Hatori, Carbon 41 (2003) 2680–2682.
[12] C. Kim, S.H. Park, W.J. Lee, K.S. Yang, Electrochim. Acta 50 (2004) 877–881.
[13] C. Kim, J.S. Kim, S.J. Kim, W.J. Lee, K.S. Yang, J. Electrochem. Soc. 151 (2004) A769–A773.
[14] C. Kim, J. Power Sources 142 (2005) 382–388.
[15] H.Y. Liu, K.P. Wang, H. Teng, Carbon 43 (2005) 559–566.
[16] C.S. Li, D.Z. Wang, X.F. Wang, J. Liang, Carbon 43 (2005) 1557–1583.
[17] K. Okajima, K. Ohta, M. Sudoh, Electrochim. Acta 50 (2005) 2227–2231.
[18] K.P. Wang, H. Teng, Carbon 44 (2006) 3218–3225.
[19] C.S. Du, J. Yeh, N. Pan, Nanotechnology 16 (2005) 350–353.
[20] Y.Z. Wei, B. Fang, S. Iwasa, M. Kumagai, J. Power Sources 141 (2005) 386–391.
[21] C.S. Du, N. Pan, Nanotechnology 17 (2006) 5314–5318.
[22] G.J. Lee, S.I. Pyun, Electrochim. Acta 51 (2006) 3029–3038.
[23] B. Fang, L. Binder, J. Power Sources 163 (2006) 616–622.
[24] S.R.S. Prabaharan, R. Vimala, Z. Zainal, J. Power Sources 161 (2006) 730–736.
[25] K.H. An, Y.H. Lee, J. Power Sources 173 (2007) 621–625.
[26] B. Fang, L. Binder, Electrochim. Acta 52 (2007) 6916–6921.
[27] S.H. Yoon, Y. Korai, I. Mochida, in: H. Marsh, F. Rodríguez-Reinoso (Eds.), Carbon Fibers and Active Carbon Fibers, Chapter 8, University of Alicante, Inc., Alicante, Spain, 2000, pp. 287–325.
[28] K. Okajima, A. Ikeda, K. Kamoshita, M. Sudoh, Electrochim. Acta 51 (2005) 972–977.
[29] B. Xu, F. Wu, S. Chen, C. Zhang, G. Cao, Y. Yang, Electrochim. Acta 52 (2007) 4595–4598.
[30] K.P. Wang, H. Teng, J. Electrochem. Soc. 154 (2007) A993–A998.
[31] E. Frackowiak, K. Metenier, V. Bertagna, F. Béguin, Appl. Phys. Lett. 77 (2000) 2421–2423.
[32] E. Frackowiak, K. Jurewicz, S. Delpeux, F. Béguin, J. Power Sources 97/98 (2001) 822–825.
[33] K.H. An, W.S. Kim, Y.S. Park, Y.C. Choi, S.M. Lee, D.C. Chung, D.J. Bae, S.C. Lim, Y.H. Lee, Adv. Mater. 13 (2001) 497–500.
[34] K.H. An, W.S. Kim, Y.S. Park, J.M. Moon, D.J. Bae, S.C. Lim, Y.S. Lee, Y.H. Lee, Adv. Funct. Mater. 11 (2001) 387–392.
[35] M. Hughes, M.S.P. Shaffer, A.C. Renouf, C. Singh, G.Z. Chen, J. Fray, A.H. Windle, Adv. Mater. 14 (2002) 382–385.
[36] M. Hughes, G.Z. Chen, M.S.P. Shaffer, D.J. Fray, A.H. Windle, Chem. Mater. 14 (2002) 1610–1613.
[37] B.J. Yoon, S.H. Jeong, K.H. Lee, H.S. Kim, C.G. Park, J.H. Han, Chem. Phys. Lett. 388 (2004) 170–174.
[38] H. Zhang, G. Cao, Y. Yang, Z. Gu, J. Electrochem. Soc. 155 (2008) K19–K22.
[39] Y. Piao, K. An, J. Kim, T. Yu, T. Hyeon, J. Mater. Chem. 16 (2006) 2984–2989.
[40] C.H. Wang, H.C. Shih, Y.T. Tsai, H.Y. Du, L.C. Chen, K.H. Chen, Electrochim. Acta 52 (2006) 1612–1617.
[41] F. Su, X. Li, L. Lv, X.S. Zhao, Carbon 44 (2006) 799–823.
[42] N. Sonoyama, M. Ohshita, A. Nijubu, H. Nishikawa, H. Yanase, J.I. Hayashi, T. Chiba, Carbon 44 (2006) 1754–1761.
[43] H.L. Zhang, Y. Zhang, X.G. Zhang, F. Li, C. Liu, J. Tan, H.M. Cheng, Carbon 44 (2006) 2778–2784.
[44] J.M. Rosolen, E.Y. Matsubara, M.S. Marchesin, S.M. Lala, L.A. Montoro, S. Tronto, J. Power Sources 162 (2006) 620–628.
[45] X.W. Chen, D.S. Su, S.B.A. Hamid, R. Schlögl, Carbon 45 (2007) 892–902.
[46] I. Alstrup, J. Catal. 109 (1988) 241–251.
[47] R.T. Yang, J.P. Chen, J. Catal. 115 (1989) 52–64.
[48] M. Shao, Q. Li, J. Wu, B. Xie, S. Zhang, Y. Qian, Carbon 40 (2000) 2961–2973.
[49] W. Li, H. Zhang, C. Wang, Y. Zhang, L. Xu, K. Zhu, Appl. Phys. Lett. 70 (1997) 2684–2686.
[50] L. Liu, Y. Qin, Z.X. Guo, D. Zhu, Carbon 41 (2003) 331–335.
[51] K.H. Liao, J.M. Ting, Carbon 42 (2004) 509–514.